Journal of Catalysis 278 (2011) 181–188

Contents lists available at ScienceDirect

Journal of Catalysis

journal homepage: www.elsevier.com/locate/jcat

Reaction pathways of ethanol electrooxidation on polycrystalline platinum catalysts in acidic electrolytes

Robert B. Kutz [1], Björn Braunschweig [1], Prabuddha Mukherjee, Rachel L. Behrens, Dana D. Dlott, Andrzej Wieckowski *

University of Illinois at Urbana-Champaign, Department of Chemistry, 600 S. Mathews Ave., Urbana, IL 61801, United States

ARTICLE INFO

Article history:
Received 25 August 2010
Revised 15 October 2010
Accepted 23 November 2010
Available online 22 January 2011

Keywords:
Ethanol
Acetic acid
Sulfate
Bisulfate
Oxidation
Platinum
Catalysis
Sum-frequency generation
SFG
Cyclic voltammetry

ABSTRACT

Ethanol electrooxidation reaction (EOR) pathways on polycrystalline platinum were studied with broadband sum-frequency generation (BB-SFG) spectroscopy and electrochemistry in unprecedented detail and under working fuel cell conditions. We present the first observation of adsorbed acetate and co-adsorbed sulfuric acid anions with SFG and a discussion of their relation to the EOR. Surface-adsorbed intermediates such as CO on Pt atop sites and acetate are observed in both H_2SO_4 and $HClO_4$ solutions. However, CO molecules on bridge sites and sulfuric acid anions are found in H_2SO_4 only. At $E < 0.5$ V vs. Ag/AgCl, CO is the predominantly adsorbed species. Increasing the potential to $E > 0.5$ V results in the oxidative removal of CO and the adsorption of acetate anions. Experiments with isotopically labeled ethanol ($^{12}CH_3{}^{13}CH_2OH$) reveal information on the carbon–carbon bond cleavage and the subsequent CO formation. In particular, the methyl fragment ($-^{12}CH_x$) produces far less ^{12}CO and suggests methyl electroreduction to methane and/or the persistence of $-CH_x$ on the Pt surface.

1. Introduction

Ethanol is one of the most promising fuels [1–3] for alcohol-based fuel cells since it can be easily produced in large quantities from plant matter, is renewable, and its complete oxidation to CO_2 provides a comparably high yield of 12 electrons per molecule. Pt model catalysts are well known as highly active but inefficient catalysts for the oxidation of small alcohols [1,2,4]. Although ethanol oxidation on Pt-based catalysts has been studied for many years, the precise reaction pathways and effects of the supporting electrolyte have yet to be fully elucidated [4,5]. Based on the observation of ethanol intermediates, very simple but incomplete models of possible reaction pathways were deduced in previous studies of ethanol electrooxidation [4,6,7]:multiple ethanol oxidation pathways occur simultaneously and often yield undesirable products and long-lived intermediates such as CO, acetaldehyde, and acetic acid. While CO and acetaldehyde can be further oxidized to CO_2 at fuel cell relevant potentials, acetic acid cannot, and therefore constitutes a 'dead end' for the reaction. Nevertheless, the persistence of adsorbed intermediates is indicative of an incomplete ethanol oxidation, and their presence significantly reduces the efficiency of ethanol-based fuel cells. In order to design more efficient fuel cells that suppress the formation of undesired intermediates such as CO and increase the selectivity of oxidation pathways toward CO_2 formation, a molecular-level understanding of the ethanol oxidation reaction (EOR) as it occurs on the catalyst surface and the effect of the supporting electrolyte is vital. For that reason, EOR has been studied previously with differential electrochemical mass spectrometry (DEMS) [8–10], infrared [4,5,11–14], Raman [15,16], and vibrational sum-frequency generation (SFG) spectroscopy [12,17]. However, Raman and IR studies can suffer from background issues and often struggle to disambiguate surface-adsorbed molecules from those diffused in the bulk solution [4,14,18]. Additionally, SFG studies of EOR have been limited so far to investigations of CO vibrational bands [12,17,19]. As a result, observations of surface-adsorbed species such as acetaldehyde [5,11,14], acetyl [4,14], and acetate [5,11,14] have, until now, been limited to linear spectroscopic techniques.

In this article, we have combined surface-specific and background-free (Section 2) SFG experiments with electrochemical experiments to study the ethanol oxidation reaction on polycrystalline Pt surfaces. We report the first SFG spectra of adsorbed acetate and co-adsorbed sulfuric acid anions during ethanol oxidation,

* Corresponding author.
E-mail addresses: dlott@scs.illinois.edu (D.D. Dlott), andrzej@scs.illinois.edu (A. Wieckowski).
[1] These authors have contributed equally to this work.

0021-9517/$ - see front matter © 2010 Elsevier Inc. All rights reserved.
doi:10.1016/j.jcat.2010.11.018

while first studies with isotopically labeled ethanol on polycrystalline Pt reveal significant new information on C–C bond cleavage and the behavior of adsorbed single-carbon fragments from ethanol oxidation on this catalyst. Our results and conclusions are expected to have far-reaching implications for new and efficient ethanol-based fuel cells.

2. Theory of sum-frequency generation

Sum-frequency generation (SFG) has been developed into a powerful vibrational spectroscopic technique for studies of surfaces and interfaces [20,21]. The sum-frequency ω_{SF} originates from a second-order non-linear process and is generated by overlapping a tunable infrared and a fixed visible laser beam in time and space at the interface of interest. The SFG intensity is proportional to the square of the second-order susceptibility $\chi^{(2)}$ [22], which vanishes within the dipole approximation in the bulk of centrosymmetric materials such as platinum and aqueous electrolytes. Surfaces and interfaces, however, necessarily break the prevailing bulk symmetry and give rise to non-vanishing $\chi^{(2)}$ contributions from the interface. The following equation describes the model used for the intensity $I(\omega_{SF})$ of the SFG signals and its dependent parameters:

$$I(\omega_{SF}) \propto \left|\chi^{(2)}_{NR} + \sum_q \frac{A_q \cdot e^{-i\theta_q}}{(\omega_{IR} - \omega_q) + i\Gamma_q}\right|^2 \cdot I(\omega_{vis}) I(\omega_{IR}) \times \exp\left[-4\ln 2 \frac{(\omega - \Omega)^2}{\Delta^2}\right] \quad (1)$$

Here, Ω and Δ refer to the frequency and bandwidth of the impinging broadband infrared (BBIR) pulse, while A_q, θ_q, ω_q, and Γ_q are amplitude, relative phase, frequency, and homogenous linewidth of the qth vibrational mode, respectively. $\chi^{(2)}_{NR}$ is the non-resonant component of the interfacial second-order non-linear susceptibility $\chi^{(2)}$. $\chi^{(2)}_{NR}$ is nearly independent of the BBIR frequency Ω and manifests as a featureless SFG contribution produced by the surface, but is highly dependent on the electronic structure of the surface [22]. Modifications such as a change in the surface oxidation or the presence of strongly adsorbed molecules such as CO can alter the interfacial electronic structure and influence $\chi^{(2)}_{NR}$ considerably. Thus, $\chi^{(2)}_{NR}$ is not a background, because it contains useful information about the electronic nature of the catalyst surface as well as a phase reference for determining the orientations of adsorbed molecular species [22–25]. Because we are mostly interested in resonant contributions of $\chi^{(2)}$ which are associated with adsorbed molecular species, we have applied a $\chi^{(2)}_{NR}$ suppression technique previously reported by Lagutchev et al. [26,27]. This technique, however, requires a compromise between a complete suppression of $\chi^{(2)}_{NR}$ and maintaining a relatively good signal-to-noise ratio of the observed vibrational bands.

3. Experimental

In all SFG and electrochemical experiments, a polished polycrystalline platinum disk (Matek) with a diameter of 6 mm was used as working electrode. A flame-annealed platinum wire (99.99%) and a commercial Ag/AgCl (BASi; MF-2052; −0.25 vs. RHE) electrode served as counter and reference electrodes, respectively. All potentials throughout this article are reported with respect to this Ag/AgCl reference. Voltammetric experiments in 0.1 M H_2SO_4 and $HClO_4$ electrolytes (double distilled, GFS Chemicals) with 0.5 M ethanol CH_3CH_2OH (99.5%) were recorded with a Princeton Applied Research (PAR 263A) potentiostat. Solutions of 0.2 M isotopically labeled ethanol were made in 0.1 M $HClO_4$ with $^{12}CH_3{}^{13}CH_2OH$ (>99%). All electrolytes used in this study were prepared with ultra-pure water ($\geqslant$18.2 MΩ, total oxidizable carbon $\leqslant$4 ppb) obtained from a Millipore Gradient A10 purification system and were thoroughly purged with Ar gas (ultra-high purity). Prior to each experiment, the Pt disk was cleaned in concentrated sulfuric acid, rinsed with ultra-pure water, and electrochemically cleaned by potential cycling between −0.28 and 1.4 V for 50 or more cycles at a sweep rate of 200 mV/s.

The BB-SFG apparatus for spectro-electrochemistry employed in this study allows for rapid acquisitions of vibrational spectra synchronized with a voltammetric scan and has been reported elsewhere [28]. Tunable broadband infrared (BBIR) pulses were generated in an optical parametric amplifier (Light Conversion; Topas) pumped by a femtosecond Ti:Sapphire laser system (Quantronix; Integra C series) at a repetition rate of 1 kHz. The BBIR pulses had pulse durations of ~120 fs, typical bandwidths $\Delta > 150\ cm^{-1}$, and pulse energies of approximately 8 and 3 μJ at frequencies Ω of 2083 and 1429 cm^{-1}, respectively. Narrow-band visible pulses with 5 μJ pulse energy and a fixed wavelength of 800 nm were generated by narrowing the fs pulses to a bandwidth of <10 cm^{-1} with a Fabry–Pérot etalon. Narrow-band visible and BBIR pulses were overlapped in time and space at an incident angle of ~60° to the normal of the Pt-electrolyte interface. Sum-frequency photons were collected with a spectrograph (Andor Technology, SR-303i-A) and a charge-coupled device (CCD) (Andor Technology, DU401A-BV). The SFG, visible, and IR photons were all p-polarized. Spectro-electrochemical experiments were carried out in a previously described [28] electrochemical cell for synchronized SFG and electrochemical experiments. In this electrochemical cell, a well-defined gap of 25 μm between the electrode surface and a CaF_2 optical window is established by a Teflon spacer of the same thickness. The electrolyte gap used in this study allows for voltammetric scans at sweep rates of $\leqslant$5 mV/s without the detriment of strong ohmic drop effects that are associated with thin-layer electrochemistry [28].

4. Results

Hanging-meniscus cyclic voltammograms (CVs) of 0.5 M ethanol electrooxidation on a polycrystalline Pt surface immersed in 0.1 M perchloric acid and 0.1 M sulfuric acid solutions are presented in Fig. 1a and b, respectively. These CVs reveal four distinct voltammetric features, which are characteristic of ethanol oxidation (three features on the anodic and one on the cathodic sweep) that are qualitatively similar in both electrolytes. The onsets of the three features on the anodic sweep appear at approximately 0.2 V, 0.4 V, and 0.75 V, respectively. The first two oxidation features are more distinct in sulfuric acid electrolyte than in the perchloric acid electrolyte. On the cathodic sweep, the onset of a reactivation feature corresponding to the reductive stripping of Pt surface oxides and subsequent ethanol oxidation is observed around 0.5–0.6 V (Fig. 1).

Chronoamperometric measurements for the electrooxidation of 0.5 M ethanol on polycrystalline Pt were performed in order to demonstrate the long-term difference in current densities produced in sulfuric and perchloric acid solutions. Fig. 2 shows the chronoamperograms (CAs) at potentials of 0, 0.5, and 0.8 V. At 0.5 V, the current density in perchloric acid reaches equilibrium at ~0.8 mA/cm^2, whereas in sulfuric acid, the equilibrium is established at a notably lower current density of ~0.6 mA/cm^2 (Fig. 2). Similarly, at 0.8 V, the current density equilibrates at ~0.3 mA/cm^2 in perchloric and slightly below ~0.2 mA/cm^2 in sulfuric acid solution. Although the current densities for each of the above electrochemical measurements are consistently lower in sulfuric acid, the overall shape of the chronoamperograms is similar in both electrolytes.

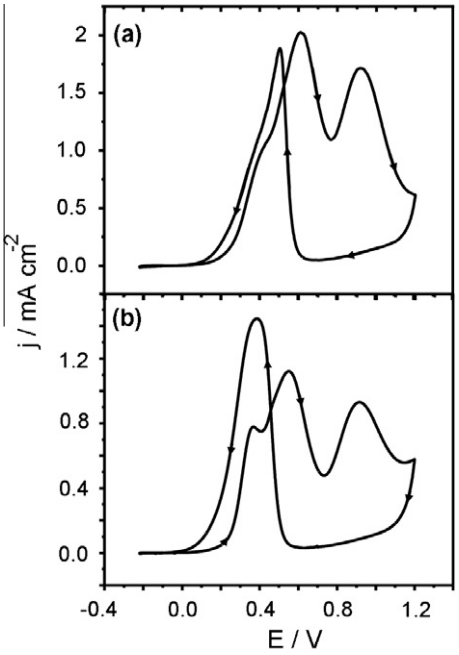

Fig. 1. Hanging-meniscus cyclic voltammograms (CVs) of a polycrystalline platinum disk in 0.5 M ethanol with (a) 0.1 M $HClO_4$ and (b) 0.1 M H_2SO_4. The CVs were recorded with a sweep rate of 5 mV/s.

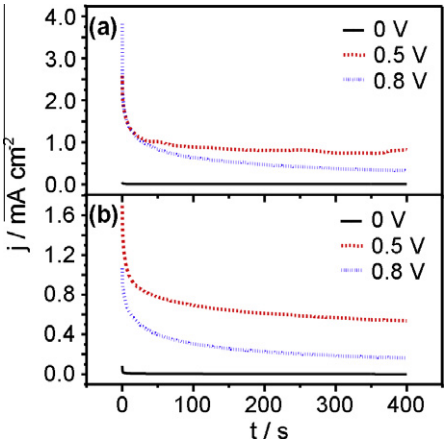

Fig. 2. Chronoamperograms of a polycrystalline Pt disk in solutions of (a) 0.1 M $HClO_4$ and (b) 0.1 M H_2SO_4 each with 0.5 M ethanol. Potentials were stepped from open-circuit conditions to the potentials indicated in the figure.

Fig. 3a and b presents two series of potentiodynamic BB-SFG spectra recorded in 0.5 M regular ethanol ($^{12}CH_3{}^{13}CH_2OH$) on a polycrystalline Pt electrode in 0.1 M $HClO_4$ and 0.1 M H_2SO_4, respectively. Vibrational bands in Fig. 3 correspond to adsorbed CO molecules which are formed by electrooxidation of ethanol. For these experiments, the BBIR frequency was tuned to ~1960 cm^{-1} to excite vibrations of CO molecules adsorbed on both Pt atop (~2080 cm^{-1}) and Pt bridge sites (1850 cm^{-1}). Vibrational bands attributable to CO molecules adsorbed on Pt atop sites are observed in both supporting electrolytes, while vibrational bands at 1850 cm^{-1} due to CO molecules adsorbed on bridge sites are present in sulfuric acid solution only.

The electrooxidation of isotopically labeled ethanol was studied with SFG in order to elucidate the formation of CO. BB-SFG spectra with the BBIR pulse centered at 2174 cm^{-1} were recorded in 0.1 M $HClO_4$ with 0.2 M isotopically labeled ethanol ($^{12}CH_3{}^{13}CH_2OH$) and are presented in Fig. 4a and b, respectively. Fig. 4a reveals two

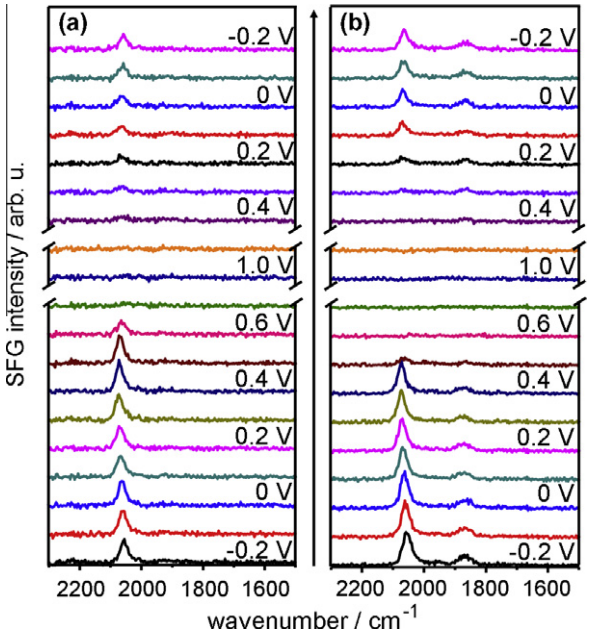

Fig. 3. Consecutive series of potentiodynamic SFG spectra of atop and bridge-bonded CO vibrational bands recorded during 0.5 M ethanol ($^{12}CH_3{}^{12}CH_2OH$) electrooxidation on a polycrystalline Pt electrode in (a) 0.1 M $HClO_4$ and (b) 0.1 M H_2SO_4. Electrode potentials *E*/*V* were as indicated in the figure. The frequency Ω of the BBIR pulse was centered at 1961 cm^{-1}.

vibrational bands at 2030 cm^{-1} and 2100 cm^{-1} that are attributable to ^{13}CO and ^{12}CO molecules adsorbed onto Pt atop sites, respectively. Note that the SFG intensity of the ^{13}CO vibrational band is much higher than the SFG intensity of the ^{12}CO vibrational band.

In order to obtain a better understanding of surface-adsorbed intermediates of ethanol and their potential dependence, we have

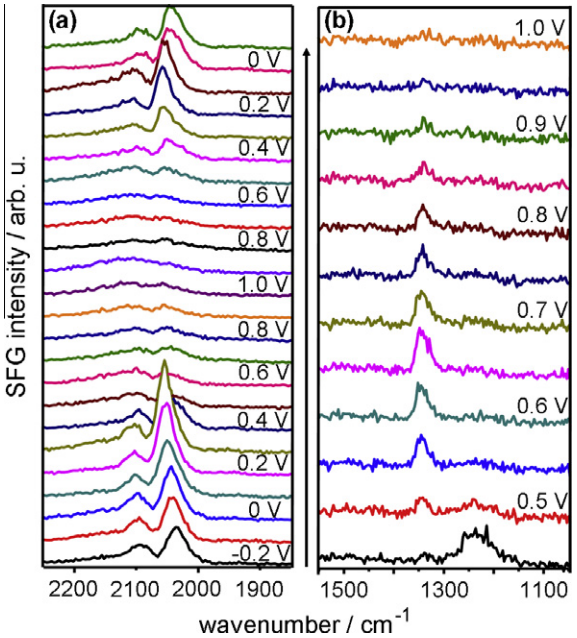

Fig. 4. Consecutive series of potentiodynamic SFG spectra of (a) $^{12}CO/^{13}CO$ and (b) symmetric carboxylate ($-^{13}COO^-$) stretching vibrations. SFG spectra were recorded during electrooxidation of 0.2 M isotopically labeled ethanol ($^{12}CH_3{}^{13}CH_2OH$) on a polycrystalline Pt electrode in 0.1 M $HClO_4$. Electrode potentials *E*/*V* are indicated in the figure. The frequency Ω of the BBIR pulse was centered at (a) 2174 cm^{-1} and (b) 1408 cm^{-1}.

fitted the vibrational bands with model functions of the interfacial second-order susceptibility $\chi^{(2)}$ and with A_q, Γ_q, ω_q, and $\chi^{(2)}_{NR}$ as adjustable parameters (see Section 2). The amplitudes A_q of the atop CO band arising from regular ethanol ($^{12}CH_3{}^{13}CH_2OH$) as a function of applied potential are shown in Fig. 5a and b for $HClO_4$ and H_2SO_4 solutions, respectively. As reported earlier, the vibrational band assigned to bridge-bonded CO is observed only in sulfuric acid electrolyte, and its amplitude is presented in Fig. 5c. The amplitudes of ^{13}CO and ^{12}CO vibrational bands are shown in Fig. 6a and b, respectively. The potential dependences of all CO vibrational band amplitudes in Figs. 5 and 6 follow very similar behavior during both the anodic and cathodic sweeps. After an initial slight increase of the CO amplitudes for potentials E from −0.2 to 0.4 V, they start to decrease rapidly for $E > 0.4$ V to negligible values for $E > 0.7$ V. The amplitudes remain negligible through the end of the anodic sweep and do not begin to increase again until potentials of $E < 0.6$ V are established during the cathodic sweep (Figs. 5 and 6).

Fig. 7 presents a comparison of SFG spectra recorded at two different BBIR frequencies during the electrooxidation of ethanol on a polycrystalline Pt surface in 0.1 M H_2SO_4. In Fig. 7a, the frequency

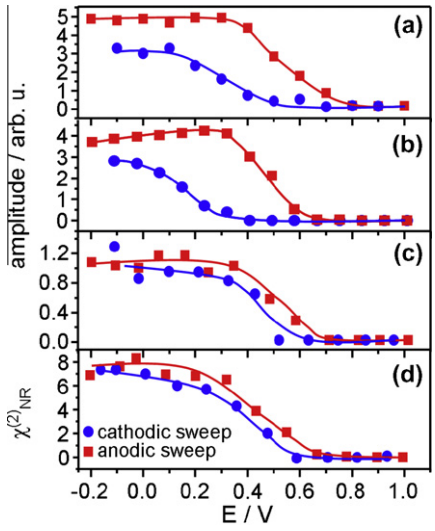

Fig. 5. (a and b) Potential dependence of modeled SFG amplitudes for atop CO atop vibrational bands (~2080 cm^{-1}) in Fig. 3 during electrooxidation of 0.5 ethanol on polycrystalline Pt in 0.1 M $HClO_4$ and 0.1 M H_2SO_4, respectively. (c) SFG amplitude of vibrational bands in Fig. 3b corresponding to bridge-bonded CO (1850 cm^{-1}) during ethanol oxidation on Pt in 0.1 M H_2SO_4. (d) Potential dependence of the non-resonant contribution $\chi^{(2)}_{NR}$ in Fig. 7 (1300 cm^{-1}). Curves are a guide to the eye.

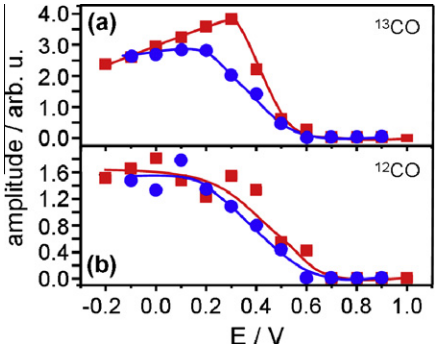

Fig. 6. Potential dependence of modeled SFG amplitudes of (a) ^{13}CO and (b) ^{12}CO vibrational bands in Fig. 4 during electroxidation of 0.5 M isotopically labeled ethanol ($^{12}CH_3{}^{13}CH_2OH$) on polycrystalline Pt in 0.1 M $HClO_4$. Curves are a guide to the eye.

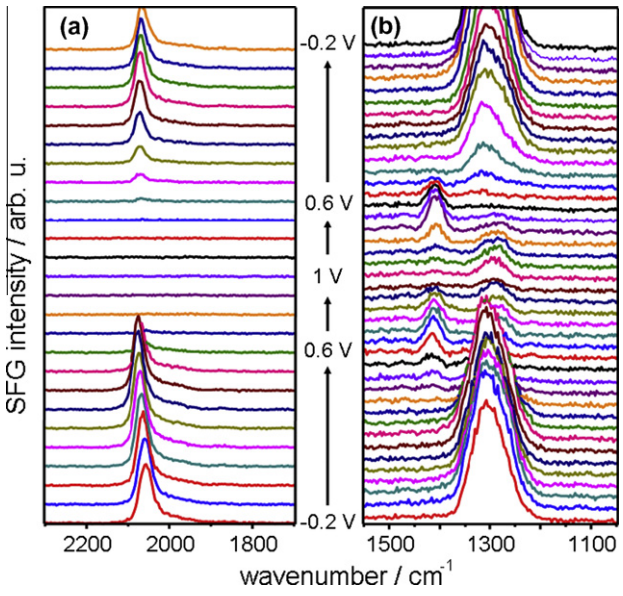

Fig. 7. Consecutive series of potentiodynamic SFG spectra recorded during 0.5 M ethanol ($^{12}CH_3{}^{12}CH_2OH$) electrooxidation on a polycrystalline Pt electrode in 0.1 M H_2SO_4. Spectra in a) show vibrational bands of ^{12}CO adsorbed on atop Pt sites, while spectra in (b) reveal (bi)sulfate and adsorbed acetate vibrational bands as well as $\chi^{(2)}_{NR}$ contributions. Electrode potentials E/V are indicated in the figure. The frequency Ω of the BBIR pulse was centered at (a) 2083 cm^{-1} and (b) 1428 cm^{-1}.

of the BBIR pulse was tuned to 2080 cm^{-1} to excite CO stretching vibrations, while in Fig. 7b, the BBIR frequency was at ~1400 cm^{-1} to probe vibrational bands attributable to adsorbed acetate and adsorbed sulfuric acid anions.

The SFG spectra in Fig. 7a show a vibrational band at ca. 2080 cm^{-1} corresponding to the adsorption of CO molecules on the Pt surface at potentials $E < 0.4$ V. CO is oxidatively removed from the Pt surface at $E > 0.4$ V which results in a dramatic decrease in the intensity of the CO vibrational band. SFG spectra at $E > 0.6$ V in Fig. 7a appear featureless and indicate the absence of adsorbed CO for these potentials. In Fig. 7b, a broad feature arises at 1300 cm^{-1} between −0.2 and 0.4 V due to a non-resonant contribution to the SFG intensity (see Section 2, Eq. (1)). The amplitude $\chi^{(2)}_{NR}$ of this non-resonant contribution is plotted as a function of electrode potential in Fig. 5d. For $E > 0.4$ V, $\chi^{(2)}_{NR}$ contributions rapidly decrease to negligible values in the anodic sweep and recover during the cathodic sweep for potentials <0.6 V (Fig. 5d). It should be noted that the potential dependence of $\chi^{(2)}_{NR}$ for both anodic and cathodic sweep follows exactly the potential dependence of the previously described CO vibrational bands (Figs. 3–6).

At potentials between 0.5 and 1.0 V with negligible $\chi^{(2)}_{NR}$ contributions and in the absence of adsorbed CO (Figs. 3–6), vibrational bands at ~1400 cm^{-1} and ~1280 cm^{-1} are observed. These bands are assigned to symmetric carboxylate ($-^{12}COO^-$) stretching vibrations of adsorbed acetate [4,29,30] (~1410 cm^{-1}) and S–O stretching vibrations of co-adsorbed sulfuric acid anions (~1280 cm^{-1}) [31–33]. The chemical identity of the adsorbed sulfuric acid anion – whether it is sulfate or bisulfate – is still a matter of considerable debate. Radiotracer and STM experiments combined with cyclic voltammetry [34,35] as well as theoretical studies [36,37] suggest that the adsorbate is sulfate rather than bisulfate. However, infrared studies contend specific adsorption of bisulfate [32,33]. Although evidence may be mounting in favor of the sulfate assignment, it is beyond the scope of this study to offer a conclusive assignment. Therefore, we refer to the adsorbed species as (bi)sulfate. Fig. 8a and b enhances the particularly interesting potential and frequency regions for acetate and (bi)sulfate adsorption in $HClO_4$ and H_2SO_4 electrolytes, respectively. In both electrolytes,

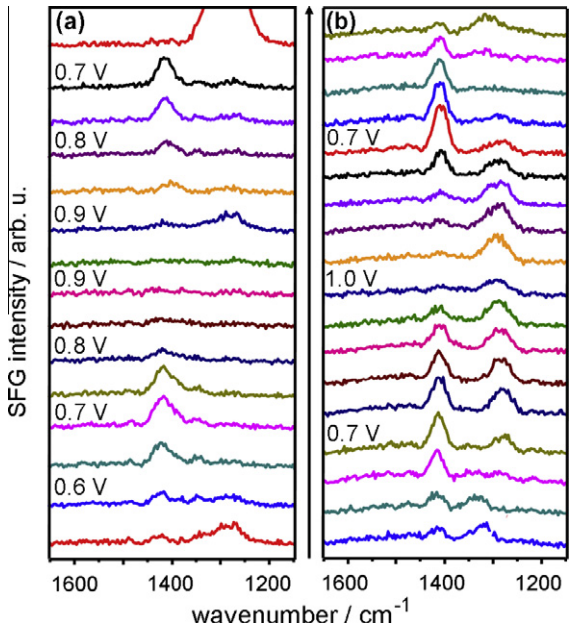

Fig. 8. Consecutive series of potentiodynamic SFG spectra of adsorbed acetate (1410 cm^{-1}) and co-adsorbed (bi)sulfate (1280 cm^{-1}) vibrational bands. Spectra were recorded during 0.5 M ethanol ($^{12}CH_3{}^{12}CH_2OH$) electrooxidation on a polycrystalline Pt electrode in (a) 0.1 M $HClO_4$ and (b) 0.1 M H_2SO_4. Electrode potentials *E*/*V* are indicated in the figure. The frequency Ω of the BBIR pulse was centered at 1429 cm^{-1}.

the acetate vibrational band at ~1410 cm^{-1} arises at $E > 0.6$ V, increases in intensity with increasing potential, reaches a local maximum and subsequently decreases to negligible intensities prior to 1.0 V. On the cathodic sweep, a similar intensity-potential profile is observed in the same potential region. The vibrational band assigned to co-adsorbed (bi)sulfate is, however, observed in H_2SO_4 electrolyte only (Fig. 8). Fig. 9 shows the amplitudes A_q of acetate and (bi)sulfate bands as a function of the applied potential. In $HClO_4$, the maximum amplitude of the acetate vibrational band is observed around 0.7 V for both anodic and cathodic sweeps (Fig. 9a) while Fig. 9b reveals acetate adsorption in dilute H_2SO_4 in a wider potential range with the maximum amplitude at a much

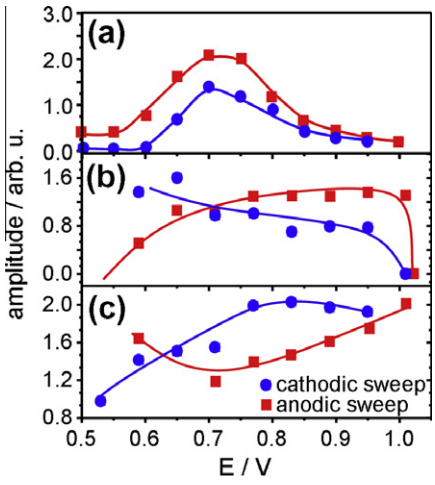

Fig. 9. (a and b) SFG modeled amplitudes of acetate vibrational bands (1410 cm^{-1}) in Fig. 8 during electrooxidation of 0.5 M ethanol ($^{12}CH_3{}^{12}CH_2OH$) on polycrystalline Pt in 0.1 M $HClO_4$ and 0.1 M H_2SO_4, respectively. (c) SFG amplitude of vibrational bands (1280 cm^{-1}) due to co-adsorbed sulfuric acid anions during ethanol oxidation in 0.1 M H_2SO_4. Curves are a guide to the eye.

Table 1
Frequencies ω_q and bandwidths Γ_q of vibrational bands used to identify adsorbates. References for these assignments are provided in the text.

Molecular species	Γ_q (cm^{-1})	ω_q (cm^{-1})
^{12}CO (atop)	28	2080–2100
^{12}CO (bridge)	40	1850
^{13}CO (atop)	30	2030
Acetate ($HClO_4$)	50	1410
Acetate (H_2SO_4)	29	1410
Acetate ($^{12}CH_3{}^{13}CH_2OH$)	25	1350
(Bi)sulfate	41	1280

higher potential of 0.9 V. The amplitude of the (bi)sulfate band increases for potentials >0.7 V and reaches its maximum at the end of the anodic sweep. During the cathodic sweep, it steadily decreases from 1 V to 0.6 V, where it is displaced by the newly formed CO adlayer.

In addition to the SFG experiments with regular ethanol ($^{12}CH_3{}^{12}CH_2OH$) in this frequency region, potentiodynamic SFG spectra shown in Fig. 4b were recorded during electrooxidation of isotopically labeled ethanol ($^{12}CH_3{}^{13}CH_2OH$) and reveal a vibrational band due to symmetric $-{}^{13}COO^-$ stretching vibrations of adsorbed and isotopically labeled acetate. A comparison of the spectra in Fig. 8a–b reveals remarkable differences in the linewidths Γ_q of the acetate vibrational bands between the two different supporting electrolytes (Table 1). In perchloric acid solution, the linewidth Γ_q is ~50 cm^{-1}, whereas in sulfuric acid, Γ_q is ~29 cm^{-1} only. The linewidth of labeled acetate shown in Fig. 4b is ~25 cm^{-1}.

5. Discussion

Potentiodynamic SFG spectra that were recorded during the electrooxidation of both regular and isotopically labeled ethanol reveal CO as the main surface-adsorbed intermediate at $E < 0.6$ V (Figs. 4 and 7). Increasing the electrode potential leads to an oxidative removal of CO and to the predominant adsorption of acetate and, in the case of a H_2SO_4 electrolyte, to the co-adsorption of (bi)sulfate anions (Fig. 8). On the basis of our spectroscopic and voltammetric observations, we propose a reaction mechanism for ethanol electrooxidation on polycrystalline Pt in Scheme 1, which will be substantiated and discussed later in the text. Scheme 1 shows oxidation of ethanol by dehydrogenation and the formation of acetaldehyde in step (a). In step (b), adsorbed acetaldehyde and adsorbed ethanol (parallel to (a)) quickly decomposes into surface-adsorbed $-CH_x$ [15] and $-CH_xO$ fragments. Note that no direct observation of a $-CH_xO$ fragment has been made so far. This is possibly due to a short lifetime of this species. It is, however, reasonable to assume that after the ethanol C–C bond is broken, a $-CH_xO$ fragment has to exist on the catalyst surface as a logical precursor to more oxidized species such as CO or CO_2. Both $-CH_x$ and $-CH_xO$

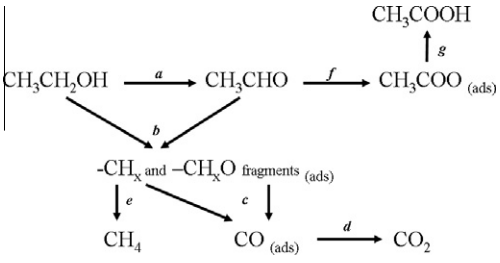

Scheme 1. Proposed reaction pathways for the electrooxidation of ethanol on a platinum surface in acidic electrolytes. Each pathway is discussed in detail in the text.

fragments can oxidize and form adsorbed CO (step (c), Scheme 1) at potentials as low as −0.2 V, although oxidation of $-CH_x$ is more difficult (Section 5.1). For electrode potentials ⩾0.4 V, the adsorbed CO molecules oxidize further to CO_2 (step (d)) (Section 5.2), which diffuses away from the catalyst surface. Not all single-carbon fragments of ethanol oxidize to CO and subsequently to CO_2, however. As shown in step (e) of Scheme 1, adsorbed $-CH_x$ fragments can be electroreduced at sufficiently low potentials to CH_4, which subsequently desorbs from the surface and diffuses in the bulk electrolyte [9,10] In the likely case that the C–C bond is not broken, acetaldehyde can oxidize to adsorbed acetate (step (f)) (Section 5.3). At this point, the adsorbed acetate can only diffuse from the surface by conversion to acetic acid (step (g)). Some authors have also reported that acetic acid can be formed on Pt(1 1 1) by a direct pathway without an acetaldehyde intermediate [8,11]. Further oxidation of acetic acid to CO_2 at fuel cell relevant potentials is not possible. Therefore, the formation of this product represents an undesirable 'dead-end' of the ethanol oxidation.

5.1. Electrooxidation of $-CH_x$ and $-CH_xO$ fragments from ethanol

The formation of CO from both $-CH_x$ and $-CH_xO$ fragments (step (c)) is confirmed by our spectroscopic data on the electrooxidation of regular (Fig. 3) and isotopically labeled ethanol ($^{12}CH_3{}^{13}CH_2OH$) (Fig. 4). In Fig. 4, CO vibrational bands of both ^{12}CO and ^{13}CO are clearly resolved and indicative of the oxidation of ethanol fragments in step (c). The coverages of ^{13}CO and ^{12}CO are not identical, however, as we observe a greater quantity of ^{13}CO formed from the $-{}^{13}CH_xO$ fragment. Because the latter fragment is already partially oxidized, further oxidation to CO is far more facile than the oxidation of $-{}^{12}CH_x$ fragments, as is evidenced by the SFG amplitudes shown in Fig. 6. Here, the amplitude of the ^{13}CO vibrational band is considerably higher than the amplitude of the ^{12}CO vibrational band. Such a difference strongly implies that the surface coverage of adsorbed ^{13}CO molecules is much higher than the surface coverage of adsorbed ^{12}CO molecules and consequently indicates that the $-{}^{12}CH_x$ fragment oxidizes to ^{12}CO to a far lesser extent. At this point, it should be noted that dipole–dipole-coupling effects arising from interactions between the different CO species could be the cause for different ^{13}CO and ^{12}CO SFG amplitudes. These coupling effects, which are well-known phenomena observed in closed-packed CO adlayers [38–40], may shift vibrational intensity from the ^{12}CO vibrational band to the ^{13}CO vibrational band and consequently may result in a virtually lower ^{12}CO intensity. If such a shift in intensity was present in Fig. 4a, then the higher amplitude observed in the ^{13}CO vibrational peak would not necessarily correspond to higher ^{13}CO coverages. However, this scenario is rather unlikely since a previous analysis of dipole-coupling effects with well-defined mixtures of $^{12}CO/^{13}CO$ on Pt(1 1 1) by Severson et al. [38] shows the opposite behavior. In their work, Severson et al. showed that for mixtures with >17% ^{12}CO, the ^{12}CO vibrational band dominated the infrared spectra. It therefore appears clear that there is an intensity shift from the ^{13}CO vibrational band to the ^{12}CO band. Thus, if our Pt catalyst has an equal coverage of ^{13}CO molecules (formed from $-CH_xO$ fragments) and ^{12}CO molecules (formed from $-CH_x$) fragments, we would expect much higher intensities of the ^{12}CO vibrational band. The fact that we see the opposite, a higher intensity of ^{13}CO vibrational bands, suggests that the surface coverage of ^{12}CO molecules is less than 17%. This is further supported in a FTIR study of ethanol ($^{12}CH_3{}^{13}CH_2OH$) oxidation on Pt(3 3 2) surfaces performed by Souza-Garcia et al. [13], where the existence of an adsorbed $-CH_x$ species is inferred by comparing the notably different intensities for $^{12}CO_2$ and $^{13}CO_2$ vibrational bands (1:3 respectively). We therefore conclude that the oxidation of adsorbed $-CH_x$ species to CO is significantly more difficult than the oxidation of $-CH_xO$ species. In addition, the difficulty of oxidizing $-CH_x$ species has been demonstrated in recent DFT model calculations [41] which show a much higher potential barrier for the oxidation of $-CH_x$ compared to $-CH_xO$ species. This leads to an accumulation of adsorbed $-CH_x$ on the catalyst surface and is supported by previous DEMS [8–10] as well as surface-enhanced Raman spectroscopy (SERS) [15] studies that report surface-adsorbed $-CH_x$ species. In fact, Abd-El-Latif et al. point out in their recent DEMS study that the remaining fraction of the $-CH_x$ species which has not been converted to CO may be oxidized in the oxygen region only [8]. Furthermore, at potentials lower than 0 V, adsorbed $-CH_x$ species can be electroreduced to methane, as shown in step (e) of Scheme 1 and supported by prior DEMS studies [9,10]. Therefore, the electrooxidation of adsorbed $-CH_x$ species to CO is expected to be less efficient and competes with the electroreduction of $-CH_x$ to CH_4 at lower potentials. Since $-CH_x$ species block available adsorption sites at fuel cell relevant potentials, oxidation of $-CH_x$ has to be considered as a serious issue in the performance of ethanol-based fuel cells.

5.2. Electrooxidation of CO from ethanol

Our spectroscopic results presented in Figs. 3–7 show that as soon as the electrode potential is increased to 0.4 V, there is a steady drop in the intensity of the CO vibrational bands, as is most clearly seen in the corresponding SFG amplitudes in Figs. 5 and 6. This drop in amplitude originates from the oxidative removal of CO from the Pt surface and the formation of CO_2 according to step (d) in Scheme 1. The dramatic decrease in CO amplitudes (Figs. 5 and 6) at potentials >0.4 V coincides with the first voltammetric feature at the same potentials Fig. 1a and b. This voltammetric feature on the anodic potential sweep corresponds largely to CO oxidation, as confirmed in prior studies by Hitmi et al. [42]. Conversely, on the cathodic potential sweep, we see the reappearance of the CO vibrational band at $E < 0.4$ V, where the Pt oxide layer is stripped and ethanol is oxidized to CO on active Pt sites. There is a slight hysteresis observed in the recovery of the CO atop vibrational band amplitude at $E < 0.4$ V on the cathodic sweep, seen in Fig. 5a and b. This is likely attributable to the slow diffusion of ethanol into the 25-μm gap and subsequent accumulation of CO on the atop Pt sites. We do not observe such a slow rise in the vibrational band amplitude at the beginning of the anodic sweep because the electrode is held at 0 V for several minutes prior to the scan, which is sufficient time to achieve saturation coverage of CO molecules on the catalyst surface. The recovery of bridge-bonded CO (Fig. 5c) is more reversible, as one might expect given that CO binds more preferentially to bridge sites when overall CO coverage is lower [43]. The $\chi^{(2)}_{NR}$ amplitude is also highly reversible. A close comparison of Fig. 5a–c with d as well as a comparison of Fig. 7a and b reveal a nearly identical potential dependence of the non-resonant contribution $\chi^{(2)}_{NR}$ (Eq. (1)) compared to the potential dependence of the CO amplitudes. In fact, Fig. 7 shows substantial changes in the contribution of $\chi^{(2)}_{NR}$ as soon as the CO adlayer starts to oxidize. We recall that the $\chi^{(2)}_{NR}$ contribution is purely electronic in origin and is caused by the non-linear response of free electrons at the metal side of the interface. The strong chemisorption of CO on most metal surfaces localizes the electrons in the adsorbate–metal bonds and decreases $\chi^{(2)}_{NR}$ contributions [23,24]. Consequently, the observed changes in $\chi^{(2)}_{NR}$ can be attributed to changes in CO coverage [25,44,45].

In addition to the potential-induced changes in CO coverage, a significant effect of the H_2SO_4 and $HClO_4$ supporting electrolyte on CO amplitudes and CO binding behavior is observed. Fig. 3 shows that the vibrational band assigned to CO molecules bound to bridge sites of the Pt electrode is observed in sulfuric acid electrolyte only. This observation is in agreement with previous

studies of ethanol electrooxidation which also report the absence of bridge-bound CO in $HClO_4$ [10,15,18,46]. The presence of CO molecules on bridge sites in vibrational SFG spectra (Fig. 3b) is indicative of an overall lower surface coverage of CO in sulfuric acid electrolyte. This conclusion is supported (i) by previous spectroscopic studies of CO on Pt surfaces which established that CO molecules bind preferentially to Pt bridge sites for low CO coverages [43] and (ii) by our electrochemical data, which show significantly lower current densities from ethanol oxidation in sulfuric acid media compared to perchloric acid media (Figs. 1 and 2). The presence of a (bi)sulfate band in our SFG spectra (Fig. 8a) confirms the specific adsorption of (bi)sulfate, while the absence of a perchlorate band at 1100 cm^{-1} in Fig. 4b [10] indicates weaker interaction between perchlorate anions and the Pt catalyst surface. These results suggest that (bi)sulfate anions block adsorption sites on the Pt surface and, therefore, inhibit ethanol oxidation which further implies a lower CO coverage and a significantly reduced reaction efficiency.

5.3. Formation of acetate species from ethanol oxidation

After the CO adlayer has been stripped from the Pt surface at potentials >0.4 V, Pt surface sites become available for other more weakly adsorbed molecular species such as acetate or (bi)sulfate. In fact, a vibrational band of adsorbed acetate arises, as shown in Figs. 7 and 8 at these potentials. The formation of acetate is represented as step (f) in the reaction Scheme 1. Additionally, we observe a pronounced effect of the supporting electrolyte on the presence and potential dependence of interfacial molecular species. Fig. 8b shows an additional vibrational band at 1280 cm^{-1} attributable to (bi)sulfate anions that is present between 0.5 and 0.9 V in sulfuric acid solution, but absent in perchloric acid (Fig. 8a). Co-adsorption of (bi)sulfate with the acetate anion widens the potential range in which both anions are adsorbed. This is most clearly seen in Fig. 9, which contrasts the potential dependence of acetate and (bi)sulfate amplitudes. In comparison to the acetate band in sulfuric acid media, the band in perchloric acid is found in a much narrower potential range of approximately 0.6–0.8 V (Fig. 9a). In addition to the different potential dependence of acetate adlayers in both supporting electrolytes, co-adsorbed (bi)sulfate confines the acetate anions on the Pt surface in a more ordered fashion. The latter is evidenced by a notably smaller linewidth Γ_q of acetate vibrational bands in sulfuric acid compared to perchloric acid solutions (Table 1). Furthermore, the decline of the acetate vibrational band amplitude on the cathodic sweep occurs between 0.5 and 0.6 V (Fig. 9), which corresponds with the voltammetric reactivation of the Pt surface via the removal of surface oxides (Fig. 1). Once this acetate vibrational band disappears and the surface oxides are removed, the CO vibrational band reappears on the cathodic sweep (Fig. 7).

The acetate anion, however, does not oxidize within the potential range in which fuel cells operate and thus either diffuses from the surface as acetic acid (step (g) in Scheme 1) or blocks Pt catalyst sites. The stabilization of acetate on the surface by (bi)sulfate co-adsorption additionally discourages the use of dilute sulfuric acid as an electrolytic medium for fuel cells, since the reaction pathway in which acetate and acetic acid are produced yields only four electrons per ethanol molecule and is therefore undesirable.

5.4. Other surface-adsorbed ethanol intermediates

In this section, we will address other possible intermediates that have been frequently reported by previous studies of ethanol electrooxidation on polycrystalline Pt surfaces. Acetaldehyde is well established as a reaction intermediate and has been identified mostly by infrared spectroscopy [17,46]. So far, it is agreed that acetaldehyde either desorbs from the Pt surface and diffuses in the bulk electrolyte or it remains adsorbed on the surface, but is quickly decomposed into CO via steps (b) and (c) of Scheme 1. Further oxidation of acetaldehyde to acetate and subsequently to acetic acid is also possible (steps (f) and (g)). Heinen et al. [4] report in their recent study of ethanol oxidation on thin-film Pt electrodes an acetyl anionic species with a vibrational band at ca. 1630 cm^{-1}. Hypothetically, this species is a long-lived surface-adsorbed intermediate of ethanol and acetaldehyde electrooxidation. As Heinen et al. point out, the observation of molecular species with vibrational bands in the frequency region of 1600–1700 cm^{-1} with linear-optical infrared spectroscopy is impaired by potential-induced background changes related to the changing molecular structure of interfacial H_2O. The broad bending mode of liquid water is at 1644 cm^{-1} [47] which renders the unambiguous identification of molecular species such as acetyl extremely difficult. One way to circumvent this problem is to substitute D_2O for H_2O for these experiments. D_2O has no strong adsorption bands for frequencies of 1600–1700 cm^{-1} and is well suited to verify possible acetyl bands. We have therefore performed additional background-free vibrational SFG experiments of ethanol oxidation in electrolytes that substituted D_2O for H_2O. We did not observe any acetyl vibrational bands at or around 1630 cm^{-1} in our broadband SFG spectra, which in fact appeared featureless.

6. Conclusion

Reaction pathways of ethanol electrooxidation on polycrystalline Pt electrodes in contact with H_2SO_4 and $HClO_4$ electrolytes were studied with broadband sum-frequency generation and electrochemistry. In this article, we report the first SFG spectra of acetate and (bi)sulfate co-adsorption during ethanol oxidation. A summary of all possible pathways substantiated by our experimental results is given in Scheme 1. Low potentials ($E < 0.4$ V) produce pathways that lead to the formation of CO, while for $E > 0.4$ V, acetate is the main surface product of ethanol electrooxidation. Our observations of ^{12}CO and ^{13}CO species from the electrooxidation of isotopically labeled ethanol ($^{12}CH_3{}^{13}CH_2OH$) show that the carbon–carbon bond of an ethanol molecule can be easily broken at low potentials. Oxidation of the resultant $-CH_x$ fragment to molecular CO is, however, far less easy than the oxidation of the complementary $-CH_xO$ fragment: while a small fraction of the $-CH_x$ species can oxidize to CO at potentials as low as −0.2 V, the majority of the $-CH_x$ species possibly undergoes electroreduction to methane at potentials lower than 0 V [10] and/or persists on the catalyst surface at higher potentials. A comparison of SFG vibrational spectra and voltammetric data reveals significant effects of the supporting electrolyte: ethanol electrooxidation in H_2SO_4 results in lower current densities, adsorption of CO onto Pt bridge sites, and co-adsorption of acetate with (bi)sulfate in a relatively wide potential range, none of which is observed in $HClO_4$.

Acknowledgments

Research described in this study was supported by the US Army Research Office under award W911NF-08-10309. DDD acknowledges partial support from the US Air Force Office of Scientific Research under award: FA9550-09-1-0163. BB gratefully acknowledges support by Professor Martin Gruebele and financial support from a Feodor Lynen fellowship of the Alexander von Humboldt Foundation.

References

[1] C. Lamy, A. Lima, V. LeRhun, F. Delime, C. Coutanceau, J.-M. Léger, J. Power Sour. 105 (2002) 283.

[2] C. Lamy, S. Rousseau, E.M. Belgsir, C. Coutanceau, J.M. Leger, Electrochim. Acta 49 (2004) 3901.
[3] F. Vigier, C. Coutanceau, A. Perrard, E.M. Belgsir, C. Lamy, J. Appl. Electrochem. 34 (2004) 439.
[4] M. Heinen, Z. Jusys, R.J. Behm, J. Phys. Chem. C 114 (2010) 9850.
[5] F. Colmati, G. Tremiliosi-Filho, E.R. Gonzalez, A. Berna, E. Herrero, J.M. Feliu, Faraday Discuss. 140 (2008) 379.
[6] S.C.S. Lai, M.T.M. Koper, Faraday Discuss. 140 (2008) 399.
[7] R.S. Ferreira, V.R. Oliveira, R. Reis, G. Maia, G.A. Camara, J. Power Sour. 185 (2008) 853.
[8] A.A. Abd-El-Latif, E. Mostafa, S. Huxter, G. Attard, H. Baltruschat, Electrochim. Acta 59 (2010) 7951.
[9] B. Bittinscattaneo, S. Wilhelm, E. Cattaneo, H.W. Buschmann, W. Vielstich, Ber. Bunsen-Ges Phys. Chem. Chem. Phys. 92 (1988) 1210.
[10] T. Iwasita, E. Pastor, Electrochim. Acta 39 (1994) 531.
[11] M.J. Giz, G.A. Camara, J. Electroanal. Chem. 625 (2009) 117.
[12] J.F. Gomes, B. Busson, A. Tadjeddine, G. Tremiliosi-Filho, Electrochim. Acta 53 (2008) 6899.
[13] J. Souza-Garcia, E. Herrero, J.M. Feliu, Chem. Phys. Chem. 11 (2010) 1391.
[14] M.H. Shao, R.R. Adzic, Electrochim. Acta 50 (2005) 2415.
[15] S.C.S. Lai, S.E.F. Kleyn, V. Rosca, M.T.M. Koper, J. Phys. Chem. C 112 (2008) 19080.
[16] Q.L. Zhong, B. Zhang, Y.M. Ding, Y.L. Liu, G.S. Rao, G.F. Wang, B. Ren, Z.Q. Tian, Acta Phys-Chim. Sin. 23 (2007) 1432.
[17] J.F. Gomes, B. Busson, A. Tadjeddine, J. Phys. Chem. B 110 (2006) 5508.
[18] F. Vigier, C. Coutanceau, F. Hahn, E.M. Belgsir, C. Lamy, J. Electroanal. Chem. 563 (2004) 81.
[19] A. Lagutchev, G.Q. Lu, T. Takeshita, D.D. Dlott, A. Wieckowski, J. Chem. Phys. 125 (2006) 154705.
[20] F.T.A. Vidal, Rep. Prog. Phys. 68 (2005) 1095.
[21] S. Roke, Chem. Phys. Chem. 10 (2009) 1380.
[22] Y.R. Shen, Nature 337 (1989) 519.
[23] H.W.K. Tom, C.M. Mate, X.D. Zhu, J.E. Cromwell, T.F. Heinz, G.A. Somorjai, Y.R. Shen, Phys. Rev. Lett. 52 (1984) 348.
[24] X.D. Zhu, W. Daum, X.-D. Xiao, R. Chin, Y.R. Shen, Phys. Rev. B 43 (1991) 11571.
[25] W. Akemann, K.A. Friedrich, U. Stimming, J. Chem. Phys. 113 (2000) 6864.
[26] H.S. Lagutchev, A.D. Dlott, J. Phys. Chem. C 111 (2007) 13645.
[27] A. Lagutchev, A. Lozano, P. Mukherjee, S.A. Hambir, D.D. Dlott, Spectrochim. Acta A 75 (2010) 1289.
[28] G.Q. Lu, A. Lagutchev, D.D. Dlott, A. Wieckowski, Surf. Sci. 585 (2005) 3.
[29] D.S. Corrigan, E.K. Krauskopf, L.M. Rice, A. Wieckowski, M.J. Weaver, J. Phys. Chem. 92 (1988) 1596.
[30] X.H. Xia, H.-D. Liess, T. Iwasita, J. Electroanal. Chem. 437 (1997) 233.
[31] B. Braunschweig, P. Mukherjee, D.D. Dlott, A. Wieckowski, J. Am. Chem. Soc. 132 (2010) 14036.
[32] M. Ito, Surf. Sci. Rep. 63 (2008) 329.
[33] A. Lachenwitzer, N. Li, J. Lipkowski, J. Electroanal. Chem. 532 (2002) 85.
[34] B. Braunschweig, W. Daum, Langmuir 25 (2009) 11112.
[35] A. Kolics, A. Wieckowski, J. Phys. Chem. B 105 (2001) 2588.
[36] N. Garcia-Araez, V. Climent, P. Rodriguez, J.M. Feliu, Electrochim. Acta 53 (2008) 6793.
[37] J.A. Santana, C.R. Cabrera, Y. Ishikawa, Phys. Chem. Chem. Phys. 12 (2010) 9526.
[38] M.W. Severson, C. Stuhlmann, I. Villegas, M.J. Weaver, J. Chem. Phys. 103 (1995) 9832.
[39] I. Villegas, M.J. Weaver, J. Chem. Phys. 101 (1994) 1648.
[40] B.N.J. Persson, M. Tushaus, A.M. Bradshaw, J. Chem. Phys. 92 (1990) 5034.
[41] G. Psofogiannakis, A. St-Amant, M. Ternan, J. Phys. Chem. B 110 (2006) 24593.
[42] H. Hitmi, E.M. Belgsir, J.M. Leger, C. Lamy, R.O. Lezna, Electrochim. Acta 39 (1994) 407.
[43] C. Lamy, Electrochim. Acta 29 (1984) 1581.
[44] I.T. Bae, J. Phys. Chem. 100 (1996) 14081.
[45] B. Pozniak, Y. Mo, I.C. Stefan, K. Mantey, M. Hartmann, D.A. Scherson, J. Phys. Chem. B 105 (2001) 7874.
[46] G.A. Camara, T. Iwasita, J. Electroanal. Chem. 578 (2005) 315.
[47] J.J. Max, C. Chapados, J. Chem. Phys. 131 (2009) 184505.